



Fixation alters the physical properties of tumor tissue that regulate nanomedicine transport

John D. Martin, Fotios Mpekris, Vikash P. Chauhan, Margaret R. Martin, Megan E. Walsh, Matthew D. Stuber, Donald M. McDonald, Fan Yuan, Triantafyllos Stylianopoulos & Rakesh K. Jain

To cite this article: John D. Martin, Fotios Mpekris, Vikash P. Chauhan, Margaret R. Martin, Megan E. Walsh, Matthew D. Stuber, Donald M. McDonald, Fan Yuan, Triantafyllos Stylianopoulos & Rakesh K. Jain (2024) Fixation alters the physical properties of tumor tissue that regulate nanomedicine transport, *Drug Delivery*, 31:1, 2430528, DOI: [10.1080/10717544.2024.2430528](https://doi.org/10.1080/10717544.2024.2430528)

To link to this article: <https://doi.org/10.1080/10717544.2024.2430528>



© 2024 The Author(s). Published by Informa UK Limited, trading as Taylor & Francis Group.



[View supplementary material](#)



Published online: 20 Nov 2024.



[Submit your article to this journal](#)



Article views: 392



[View related articles](#)



[View Crossmark data](#)

Fixation alters the physical properties of tumor tissue that regulate nanomedicine transport

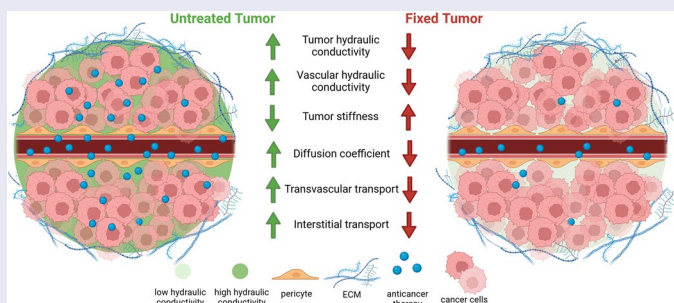
John D. Martin^{a#}, Fotios Mpekris^{b#}, Vikash P. Chauhan^c, Margaret R. Martin^d, Megan E. Walsh^e, Matthew D. Stuber^f, Donald M. McDonald^g, Fan Yuan^h, Triantafyllos Stylianopoulos^b and Rakesh K. Jainⁱ

^aMateria Therapeutics, Las Vegas, NV, USA; ^bCancer Biophysics Laboratory, Department of Mechanical and Manufacturing Engineering, University of Cyprus, Nicosia, Cyprus; ^cKoch Institute for Integrative Cancer Research, Massachusetts Institute of Technology, Cambridge, MA, USA; ^dDepartment of Computer Science, Tufts University, Medford, MA, USA; ^eDepartment of Chemical Engineering, Carnegie Mellon University, Pittsburgh, PA, USA; ^fProcess Systems and Operations Research Laboratory, Department of Chemical and Biomolecular Engineering, University of Connecticut, Storrs, CT, USA; ^gHelen Diller Family Comprehensive Cancer Center, Department of Anatomy, University of California, San Francisco, CA, USA; ^hDepartment of Biomedical Engineering, Duke University, Durham, NC, USA; ⁱEdwin L. Steele Laboratories, Department of Radiation Oncology, Massachusetts General Hospital, Harvard Medical School, Boston, MA, USA

ABSTRACT

To have the desired therapeutic effect, nanomedicines and macromolecular medications must move from the site of injection to the site of action, without having adverse effects. Transvascular transport is a critical step of this navigation, as exemplified by the Enhanced Permeability and Retention (EPR) effect in solid tumors, not found in normal organs. Numerous studies have concluded that passive, diffusion- and convection-based transport predominates over active, cellular mechanisms in this effect. However, recent work using a new approach reevaluated this principle by comparing tumors with or without fixation and concluded the opposite. Here, we address the controversy generated by this new approach by reporting evidence from experimental investigations and computer simulations that separate the contributions of active and passive transport. Our findings indicate that tissue fixation reduces passive transport as well as active transport, indicating the need for new methods to distinguish the relative contributions of passive and active transport.

GRAPHICAL ABSTRACT



ARTICLE HISTORY

Received 18 July 2024
Revised 6 November 2024
Accepted 11 November 2024





KEYWORDS

cancer nanomedicine; drug delivery; hydraulic conductivity; mouse model; computational model


Introduction

Transvascular transport, the movement of molecules and particles from blood vessels into tissues, is a critical step regulating the efficacy of cancer nanomedicines and macromolecular therapies (Jain & Stylianopoulos, 2010). The biodistribution and intratumor delivery of drugs are thought to strongly influence antitumor effects. Furthermore, understanding the kinetics and mechanism of transport can guide the design of

nanoparticles' physicochemical properties and controlled release. Transvascular transport has been studied in many contexts, with early studies providing evidence that transvascular transport of molecules and nanoparticles in tumors occurs primarily by passive transport involving diffusion and/or convection (Gerlowski & Jain, 1986; Matsumura & Maeda, 1986; Yuan et al., 1993, 1995, 1996; Fukumura et al., 1997; Hobbs et al., 1998; Cabral et al., 2011; Chauhan et al., 2012;

CONTACT Rakesh K. Jain  rjain@mgh.harvard.edu  Edwin L. Steele Laboratories, Department of Radiation Oncology, Massachusetts General Hospital, Harvard Medical School, Boston, MA, USA; Triantafyllos Stylianopoulos  tstylian@ucy.ac.cy  Cancer Biophysics Laboratory, Department of Mechanical and Manufacturing Engineering, University of Cyprus, Nicosia, Cyprus

[#]Equal contributions.

 Supplemental data for this article can be accessed online at <https://doi.org/10.1080/10717544.2024.2430528>.

© 2024 The Author(s). Published by Informa UK Limited, trading as Taylor & Francis Group.

This is an Open Access article distributed under the terms of the Creative Commons Attribution-NonCommercial License (<http://creativecommons.org/licenses/by-nc/4.0/>), which permits unrestricted non-commercial use, distribution, and reproduction in any medium, provided the original work is properly cited. The terms on which this article has been published allow the posting of the Accepted Manuscript in a repository by the author(s) or with their consent.

Lu et al., 2020). Active transport occurs in neuropilin-1/iRGD peptide regulated transport (Liu et al., 2017), albumin transport by the endothelial gp60 receptor (Desai et al., 2006), and multiple other contexts. Recent studies have sought to reevaluate the extent to which active transport processes, as in trafficking through living cells, contribute to the transport of nanoscale species such as nanoparticles. The Zombie model was developed to quantify the contribution of active transport (Sindhwani et al., 2020). This model involves fixation of entire mice by cross-linking fixatives, with the aim of stopping cellular activity and thereby eliminating active transport. Transvascular transport is then compared in live and Zombie model mice. Transport in living mice is the sum of active and passive processes, whereas transport in the Zombie model is posited to represent only passive transport. The model has since been used in several studies to parse the contributions of passive and active transport in murine tumors (Chen et al., 2023; Zhu et al., 2023). The critical assumption made in these studies is that passive transport is unaffected by cross-linking fixatives. However, the rationale and justification for this assumption have been questioned (Crist et al., 2021; Skotland & Sandvig, 2021; Dasgupta et al., 2024). Here, we sought to address this controversy by determining how cross-linking fixatives affect the relative contribution of passive forces to interstitial and transvascular transport in tumor tissue.

Materials and methods

Cell culture

4T1 (ATCC[®] CRL-2539[™]) mouse breast adenocarcinoma cell line was purchased from ATCC. The cells were maintained at 37°C/5% CO₂ in Roswell Park Memorial Institute medium (RPMI-1640, LM-R1637, biosera) supplemented with 10% fetal bovine serum (FBS, FB-1001H, biosera) and 1% antibiotics (A5955, Sigma).

Syngeneic tumor model

An orthotopic model for murine mammary tumors was generated by implantation of 5×10^4 4T1 cancer cells in 40 μ l of serum-free medium into the third mammary fat pad of 6–8-week-old BALB/c female mice. Ten (10) mice were used for this experiment. 4T1 tumors were excised when they reached an average size of 200 mm³ (12 days post implantation), washed in 1x PBS for 20 minutes, fixed by immersion in 4% PFA overnight at 4°C and washed again in 1x PBS for 20 minutes before the mechanical testing experiment.

Calculation of hydraulic conductivity

The standard biphasic model of soft tissue biomechanics used (Mow et al., 1980) accounted for both the solid components (cells and extracellular matrix) and the fluid phase (interstitial fluid) of the tumor (Stylianopoulos et al., 2013). The solid phase stress, σ^s , was modeled as a neo-Hookean material with elastic modulus values derived from stress-strain

experiments, assuming a Poisson's ratio of $\nu=0.45$ (Stylianopoulos et al., 2013). The fluid phase was assumed to be inviscid (i.e. ideal fluid) with the fluid stress given by $\sigma^f = -p\mathbf{I}$, where p the interstitial fluid pressure. The interstitial fluid velocity was governed by Darcy's law, stating that the velocity is proportional to the pressure gradient of the interstitial fluid, with the hydraulic conductivity of the interstitial space serving as the proportionality constant, i.e. $v^f = -K_{th}\nabla p$. The governing equations are: the momentum balance: $\nabla \cdot (\sigma^s - p\mathbf{I}) = 0$ and the mass conservation $\nabla \cdot v^s - K_{th}\nabla^2 p = 0$. The model was implemented in the finite elements' commercial software COMSOL Multiphysics (COMSOL, Inc., Burlington, MA). The stress relaxation experiment was simulated using the mathematical model and model predictions were fitted to the experimental data by varying the hydraulic conductivity, K_{th} , of the tumor interstitial space (Papageorgis et al., 2017; Polydorou et al., 2017). From the fitting, the value of the hydraulic conductivity was determined.

Quantification of elastic modulus and hydraulic conductivity

Tumors were excised from animals and tissue specimens of $3 \times 3 \times 2$ mm (length \times width \times thickness) were loaded on a high precision mechanical testing system (Instron, 5944, Norwood, MA, USA). For the measurement of the elastic modulus, the specimens were placed between two platens and were compressed to a final strain of 20% with a strain rate of 0.05 mm/min. The elastic modulus was calculated from the initial slope of the stress vs strain curve. For the determination of the hydraulic conductivity, tumor tissue specimens underwent three cycles of compressive stress followed by a relaxation period of 10 minutes. In the first cycle, the specimen was compressed by 10% for 1 minute and then was held for 10 minutes, whereas for the other two cycles the specimen was compressed by 5%. Subsequently, the hydraulic conductivity was calculated by fitting the experimental stress relaxation data with a biphasic biomechanical model of soft tissues (Mpekris et al., 2015; Angeli & Stylianopoulos, 2016), using the method described previously (Papageorgis et al., 2017; Polydorou et al., 2017).

Statistical analysis

GraphPad Prism 9 was used for statistical analyses. The experimental data are presented as the mean \pm SE. Unpaired two-sided Student's t-test was used for comparison between groups. Statistical significance was defined as p -values < 0.05 .

Mathematical modeling of nanoparticle accumulation

We used a previously developed and validated mathematical model that describes fluid and macromolecule transport in tumors (Jain & Baxter, 1988; Baxter & Jain, 1989, 1990, 1991a,b). The delivery of the nanoparticles (c_n -nanoparticle concentration) is given by the interstitial transport equation below:

$$\frac{\partial c_n}{\partial t} + \nabla \cdot (c_n \mathbf{v}^f) = D_n \nabla^2 c_n + Q_{sta}, \quad (1)$$

where D_n is the diffusion coefficient of the differently sized nanoparticles in the tumor interstitial space according to a previous study (Pluen et al., 2001) and \mathbf{v}^f is the fluid velocity, which depends on the interstitial hydraulic conductivity K_{th} and is given by Darcy's law (Byrne & Preziosi, 2003):

$$\mathbf{v}^f = -k_{th} \nabla p_i. \quad (2)$$

Q_{sta} denotes the rate of transport of the drug across the tumor vessel wall and is given by Baxter & Jain (1989):

$$Q_{sta} = P \cdot S_v (C_{iv} - c_n) + L_p S_v (p_v - p_i) (1 - \sigma_f) C_{iv}, \quad (3)$$

where C_{iv} is the vascular concentration of the drug and is given by the same equation that Sindhvani et al. used (Sindhvani et al., 2020), S_v is the vascular density (value adapted from Sindhvani et al.), L_p is the hydraulic conductivity of the vessel wall, p_v is the vascular pressure, p_i is the interstitial fluid pressure, σ_f is the reflection coefficient and P is the permeability of blood vessels to the drug, given by Deen (1987):

$$P = \frac{\gamma H D_0}{L}, \quad (4)$$

where γ is the fraction of vessel wall surface area occupied by pores, H is a parameter governing hydrodynamic interactions between the nanoparticles and the pores of the vessel walls defined later, L is the thickness of the vessel walls and D_0 is the diffusion coefficient of a particle in free solution at 310K, given by the Stokes-Einstein relationship

$$D_0 = \frac{K_b T}{6\pi\eta r_s}, \quad (5)$$

where K_b is the Boltzmann constant, T is temperature, η is the viscosity of blood and r_s the radius of the diffusing particle.

The normalized transvascular flux (Yuan et al., 1994, 1995; Chauhan et al., 2012) was calculated using:

$$\frac{J_t}{S_v (C_v - c_n)} = P_{eff} = \lim_{\tilde{t} \rightarrow 0} \frac{\partial}{\partial \tilde{t}} \int_{\tilde{r}=\tilde{R}}^{\infty} c_n \tilde{r} d\tilde{r} (C_v - c_n) \tilde{R} \quad (6)$$

where J_t is the transvascular flux, C_v is the concentration of the probe outside the vessel, P_{eff} is the effective permeability, \tilde{t} is the time after the initial image, \tilde{r} is the distance from the vessel central axis, and \tilde{R} is the vessel radius at that point along the vessel.

The hydraulic conductivity of the vessel wall was calculated from the expression (Deen, 1987):

$$L_p = \frac{\gamma r_0^2}{8\eta L}, \quad (7)$$

where r_0 is the pore radius. The pore radius was evaluated from the value of effective permeability according to a previous study (Deen, 1987).

The reflection coefficient is given by the equation (Deen, 1987):

$$\sigma_f = 1 - W, \quad (8)$$

where H and W describe hydrodynamic and electrostatic interactions. Ignoring electrostatic interactions, H and W are reduced to Deen (1987):

$$H = \frac{6\pi F}{K_t} \quad (9)$$

$$W = \frac{F(2-F)K_s}{2K_t}, \quad (10)$$

where F is the partition coefficient (Deen, 1987):

$$F = (1 - \lambda)^2 \quad (11)$$

and λ is the ratio of the drug size to the vessel wall pore size.

The coefficients K_s and K_t are determined by Deen (1987):

$$\left(\frac{K_t}{K_s} \right) = \frac{9}{4} \pi^2 \sqrt{2} (1 - \lambda)^{-5/2} \left[1 + \sum_{n=1}^2 \left(\frac{a_n}{b_n} \right) (1 - \lambda)^n \right] + \sum_{n=0}^4 \left(\frac{a_{n+3}}{b_{n+3}} \right) \lambda^n. \quad (12)$$

Solution strategy

To compare the experimental data of the accumulation of gold nanoparticles in normal mouse tumors and zombie mouse tumors with the mathematical model predictions of passive transport, the following approach was taken. The geometry of the model consists of a spherical tumor domain embedded at the center of a cubic host tissue domain, which is two orders of magnitude larger than the tumor to avoid any boundary effects on the growth of the tumor (Supplementary Figure 1). Due to symmetry, only one eighth of the geometry was considered. To this end, equations were solved simultaneously using the commercial finite element software COMSOL Multiphysics (COMSOL, Inc., Burlington, MA, USA). Values for the model parameters are provided in Supplementary Table 1. The boundary conditions for the concentration of the nanoparticles at the interface of the tumor and the normal tissue were applied automatically by the software; the remaining boundary conditions are shown in Supplementary Figure 1.

For the comparisons with the zombie model data, the nanoparticle concentration in the tumor at the appropriate times relative to the values used by Sindhvani et al. (Sindhvani et al., 2020) was computed after varying the interstitial and vessel wall hydraulic conductivities. Please refer to Ref. (Sindhvani et al., 2020) for characterization of the gold nanoparticles.

Results

Hydraulic conductivity is a critical material property that characterizes passive transport through tissue. Reduced

hydraulic conductivity of the microvascular wall and interstitial space impairs the transport and accumulation of macromolecular and nanoscale medicines in tumors (Netti et al., 2000; Chauhan et al., 2013; Papageorgis et al., 2017). Because nanoparticle concentrations were measured in the interstitial space of tumors to estimate transvascular transport in the Zombie model, we asked how sensitive nanoparticle concentrations in tumors are to hydraulic conductivity. We applied a mathematical model to simulate diffusion and convection of nanoparticles across the vessel wall and in the interstitial space as a function of hydraulic conductivity (Jain & Baxter, 1988; Baxter & Jain, 1989; Chauhan et al., 2012). We used nanoparticles with the same dimensions as those originally used to validate the Zombie model (i.e. 15 nm, 50 nm, and 100 nm) (Sindhvani et al., 2020). Based on the mathematical model's predictions, the relative concentration of the 15 nm NP would be most affected by reduced hydraulic conductivity (Figure 1(A-C)). Conceptually, the transport of a particle much, much smaller than the pore it is transporting through would be unaffected by a small change in the pore (Chauhan et al., 2012). Similarly, the transport of a particle approaching the size of the pore is already hindered, so small changes in

the pore size do not affect transport much. However, there is a size range of particles between these two regimes where the transport of the nanoparticle varies with small changes in the pore. Additionally, the mathematical model predicts that, in certain circumstances, an 80% reduction in either vascular or interstitial hydraulic conductivity alone can eliminate nanoparticle accumulation (Figure 1(A-C)). If both vascular and interstitial hydraulic conductivities are reduced, a smaller reduction can lead to a larger decrease in nanoparticle accumulation.

Considering that our simulations indicate that hydraulic conductivity is critical in regulating transvascular transport, we next queried whether tissue fixation by immersion in paraformaldehyde (PFA), as used in the Zombie model, affects hydraulic conductivity. Fixation can decrease interstitial hydraulic conductivity by 50% in the eye sclera and 75% in the cornea (Stewart et al., 2009a, 2009b), but whether such changes occur in tumors is unclear. To investigate this, we determined the hydraulic conductivity of 4T1 murine breast tumors removed from five un-fixed control mice and five fixed mice. On average, fixation reduced the hydraulic conductivity by 78% (Figure 2(A,B)), which would severely limit

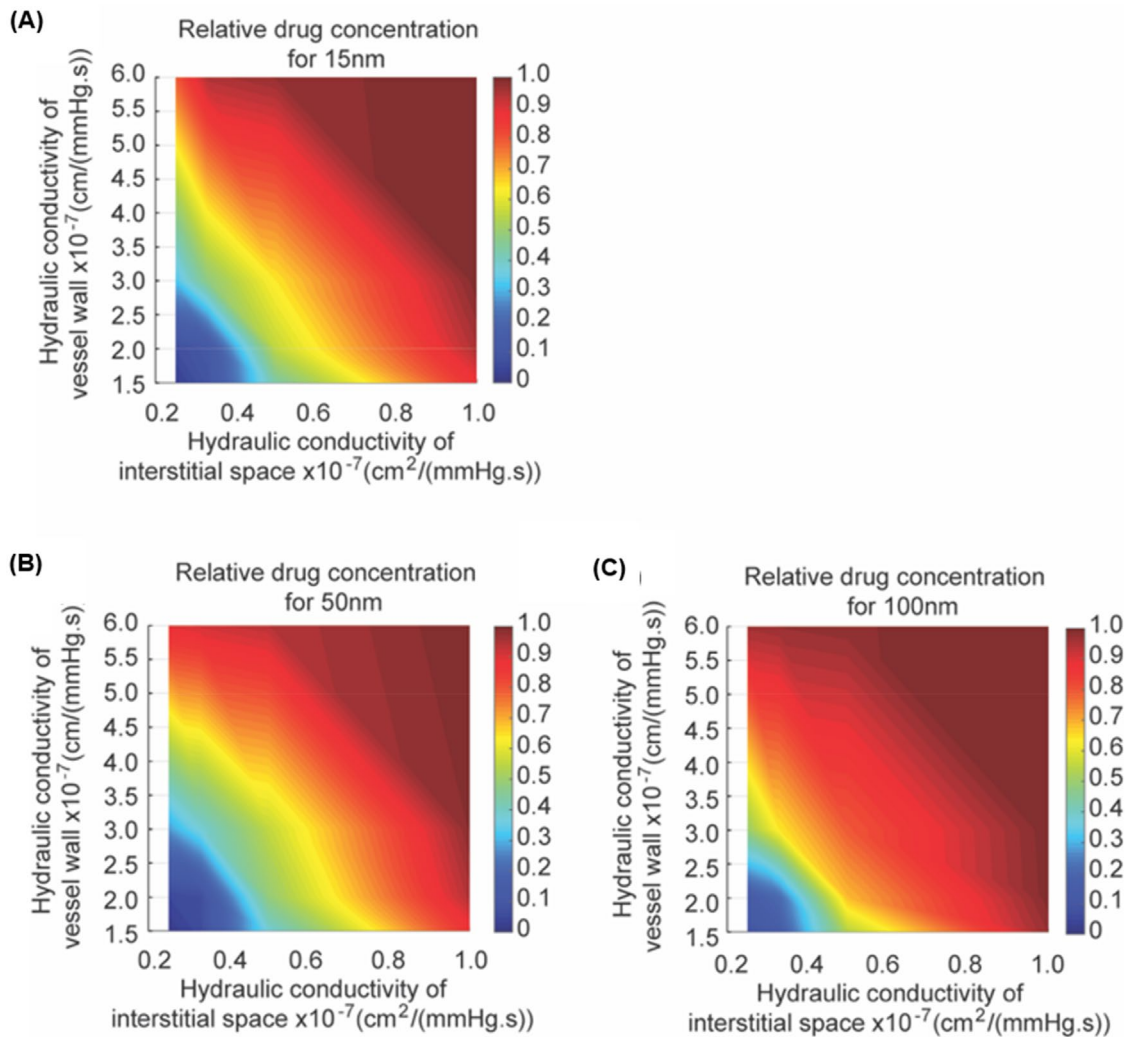


Figure 1. Nanoparticle tumor accumulation is sensitive to vessel wall and interstitial hydraulic conductivities. (A-C) Graphs of relative drug concentration accumulated over time and spatially averaged (presented as the ratio of control to zombie accumulation) as a function of hydraulic conductivities of the vessel wall (vertical axis) and interstitial space (horizontal axis) for (A) 15 nm, (B) 50 nm and (C) 100 nm.

nanoparticle accumulation, consistent with previous reports (Sindhvani et al., 2020). This suggests that passive transport reflected by hydraulic conductivity is greatly reduced by tissue fixation, in contrast to the assumption underlying the use of the Zombie model approach.

Diffusivity through tissue is another parameter that affects nanoparticle accumulation resulting from passive transport (Ramanujan et al., 2002). Previous studies reported that the diffusivity through type I collagen gels *in vitro* decreased 20% after fixation (Sindhvani et al., 2020). We sought to determine whether the diffusivity in tumor tissue is similarly altered after tissue fixation. As diffusivity and tissue stiffness are inversely correlated in tumors and other organs (Netti et al., 2000; Evans & Quinn, 2005), we measured the elastic modulus using an unconfined compression experimental protocol. Our data revealed that tumor tissue stiffness (i.e. elastic modulus) increased 2.0-fold after fixation (Figure 2(C,D)), which indicates that tissue fixation likely reduces nanoparticle diffusivity.

Finally, we asked whether these fixation-induced changes in tissue properties that regulate passive transport could lead to the changes in nanoparticle accumulation previously observed, in the absence of a contribution of active transport (Sindhvani et al., 2020). Again, we used a mathematical model and assumed a 20% reduction in diffusivity, as was measured in collagen gels, to account for tissue fixation (Sindhvani et al., 2020). Our simulations indicate that 67% reduction in both vascular and interstitial hydraulic conductivities after tissue fixation would decrease nanoparticle concentrations to an extent matching the experimental data

reported from studies using the Zombie model (Figure 3). Thus, our model simulations provide further evidence for decreased passive transport and nanoparticle accumulation in tumors after tissue fixation when active transport has been eliminated.

Discussion

In our study, we measured tissue stiffness and hydraulic conductivity in tumor tissue fixed by PFA, which induces covalent cross-linking through a methylene bridge between its aldehyde group and a nitrogen atom with another atom in proteins, thereby destroying and stiffening cellular structures and extracellular matrix (Kim et al., 2017). We used mathematical models to explore the relationship between vascular and interstitial hydraulic conductivities and accumulation of variously sized nanoparticles. As the pore sizes of the vessel wall and interstitial space decrease toward the size of the nanoparticle, the hydrodynamic hindrances to convective and diffusive transport rise.

One limitation of our study is that the hydraulic conductivity was measured as a bulk property and cannot be measured separately for interstitial tissue and microvessels. Previous studies using electron microscopy documented that PFA does not eliminate endothelial cell defects and gaps in tumor blood vessels (Hashizume et al., 2000). Nonetheless, tumors feature heterogenous microvasculature basement membrane that can be unusually thick or entirely absent (Baluk et al., 2003). In either scenario, there could be higher density of collagen polypeptides for PFA cross-linking. If so,

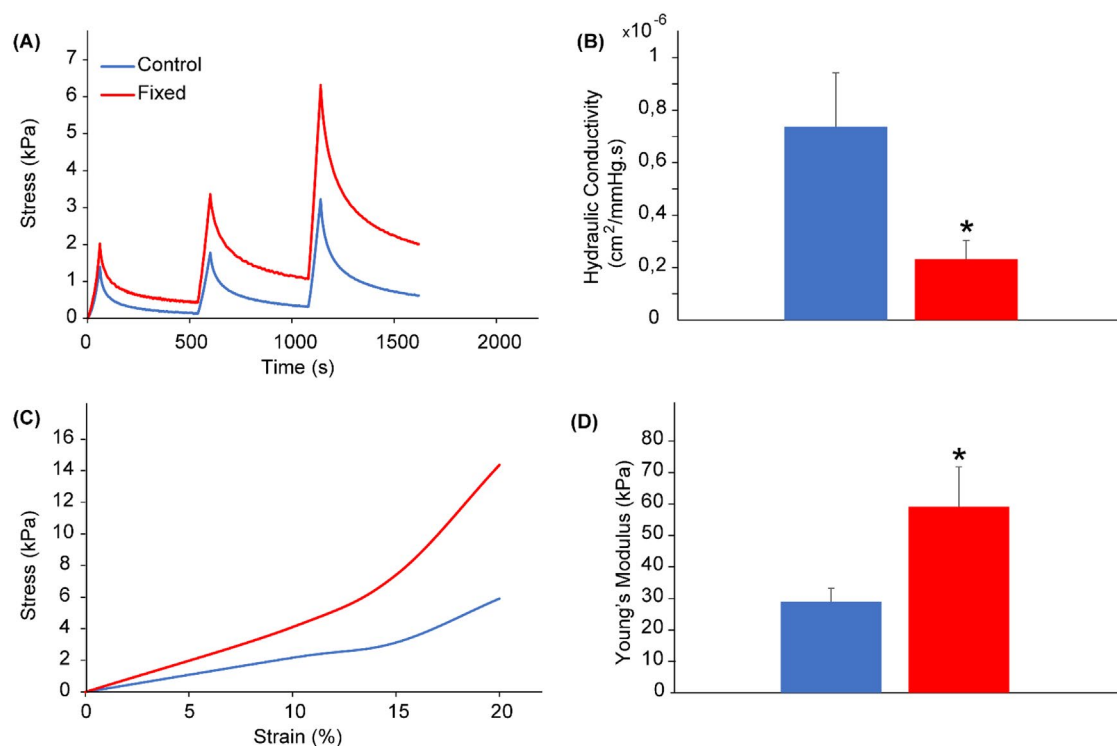


Figure 2. Increase in stiffness and decrease in tumor hydraulic conductivity induced by paraformaldehyde fixation of tumor tissues. (A) Illustration of compressive stress relaxation vs time curves of fixed (red) and unfixed (blue) 4T1 breast tumor tissues *ex vivo* subjected to stress relaxation. (B) Tumor hydraulic conductivity calculated from the stress relaxation curves. (C) Illustration of stress vs strain relationships. (D) The elastic modulus of tumors measured from the initial slope of the stress-strain curves. Bars: mean value; error bars: SEM; * $p < 0.05$; $n = 5$.

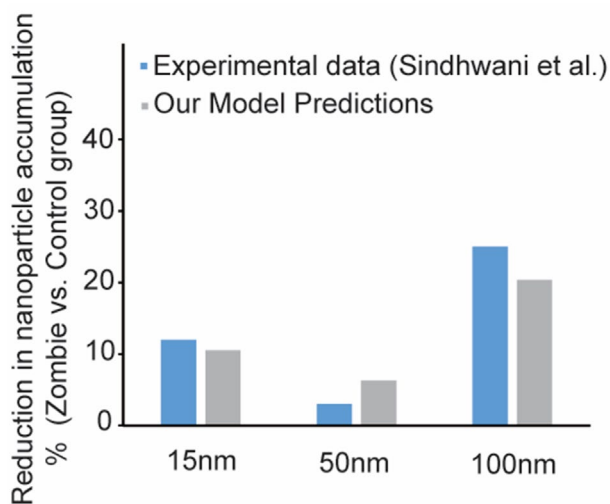


Figure 3. Comparison between experimental data and computational simulations of the ratio of nanoparticle accumulation in zombie group to control group for each size of nanoparticles. The simulated accumulation is at 4 hours for the 15-nm and 50-nm particles and at 1 hour for the 100-nm particles post intravenous administration. The nanoparticle accumulation predicted by the model simulating the experimental procedure (gray) is consistent with the measured data of the 'zombie model' (blue). Our model was developed based on passive transport and accounting for reduced diffusivity and hydraulic conductivity caused by tissue fixation.

PFA might reduce porosity of the vascular basement membrane resulting in decreased vascular hydraulic conductivity. As a result, the reflection coefficient would increase, together increasing the contribution of oncotic pressure. Based on this assumption, we estimate the change in vascular hydraulic conductivity to be roughly equivalent to the change in the interstitial component. Another limitation of our study is that, while we measured tumor tissue stiffness after fixation to test the validity of *in vitro* measurements of changes in diffusivity, we used diffusivity values from previous *in vitro* studies (Sindhvani et al., 2020), because we did not measure diffusivity. Given the synergistic interaction of interstitial and vascular hydraulic conductivities, reflection coefficient and diffusivity, the effect of fixation on passive transport is likely to be even greater than estimated here.

We conclude that tissue fixation greatly affects key parameters that regulate passive transvascular transport. Results of our mathematical models predict that reduction in either interstitial or vascular hydraulic conductivity can impair nanoparticle concentrations, the main parameter measured in the Zombie model. Further, our models indicate that reductions in both hydraulic conductivities could synergistically reduce nanoparticle accumulation. We found experimentally that fixation, an essential feature of the Zombie model, resulted in 78% reduction in interstitial hydraulic conductivity of tumor tissue and is assumed to result in similar reductions in vascular hydraulic conductivity. Additionally, the elastic modulus of tumor tissue was increased after fixation, supporting previous findings from *in vitro* collagen gels, where diffusivity was reduced by 20% after fixation. Our simulations predict that the reduced nanoparticle accumulation observed experimentally would occur with a 67% reduction in hydraulic conductivity, independent of the consequences of eliminating active mechanisms by fixation. These findings suggest

that the Zombie model does not in fact enable measurement of the relative contributions of active and passive transport, but rather reveals the effects of tissue fixation on both passive transport and active transport. Although nanoparticle extravasation observed after fixation in the Zombie model is evidence of passive transport, the absence of extravasated nanoparticles in fixed tumors is not proof of absence of passive leakage. Use of contemporary immunoelectron microscopy coupled with super resolution and confocal imaging could extend the understanding of the barrier properties of tumor blood vessels to nanoparticles. Yet, new strategies using intravital microscopy, such as imaging transport in tumors at low temperatures to slow or stop active transport, should be developed. Our findings underscore the need for new experimental methods to distinguish active and passive transport in tumors.

Author contributions

All authors contributed to conceptualization, methodology, validation, formal analysis, investigation, resources, data curation, writing – review and editing and visualization of the article. John D. Martin was responsible for writing the original draft. John D. Martin, Triantafyllos Stylianopoulos and Rakesh K. Jain were responsible for supervision and project administration. Fan Yuan, Donald M. McDonald, Triantafyllos Stylianopoulos and Rakesh K. Jain were responsible for funding acquisition.

Ethical approval statement

Mice were purchased from the Cyprus Institute of Neurology and Genetics and *in vivo* experiment was conducted in accordance with the animal welfare regulations and guidelines of the Republic of Cyprus and the European Union (European Directive 2010/63/EE and Cyprus Legislation for the protection and welfare of animals, Laws 1994–2013) under a license acquired and approved (CY/EXP/PR.L14/2019) by the Cyprus Veterinary Services committee, the Cyprus national authority for monitoring animal research for all academic institutions. The mice were housed at the Transgenic Mouse Facility (TMF) of the Cyprus Institute of Neurology and Genetics in Nicosia, Cyprus, and were looked after by a team of full-time animal caretakers. The TMF contains a fully functional barrier containment facility, where the mice were housed. Further, TMF is manufactured to a 'clean room' facility standard meeting biological safety level (BSL)-3 requirements. Animals were kept in specific pathogen free conditions, according to regulations contained in the Cyprus Law N.55 (I)/2013, which is fully harmonized to the EU Directive 2010/63/EU. The Facility is licensed by the Cyprus Veterinary Services (C.EXP.101). In order to maintain the colony under defined flora conditions, mice were changed under sterile conditions in a laminar flow hood. All the bedding and water for the mice was sterilized by autoclaving. Special care was taken to minimize potential pain, suffering or distress, and enhance animal welfare for the animals still used. Mice were anesthetized during tumor implantation or prior to euthanasia with Avertin (250 mg/kg), and placed on a heating pad to maintain body temperature at 37°C. Mice were observed daily for their level of activity and for normal eating, drinking and grooming behavior. Pain reducing agents (i.e. ibuprofen) were administered intraperitoneally occasionally to reduce pain symptoms. The maximal tumor burden of 1200 mm³, as approved by the ethics committee, was not exceeded. Mice were euthanized using cervical dislocation. *In vivo* study was used to support mathematical model findings that fixation alters the physical properties of tumor tissue leading to regulation of nanomedicine transport. Ten (10) mice were used in this study. The authors have adhered to the ARRIVE guidelines.

Disclosure statement

RKJ received consultant fees from Cur, DynamiCure, SynDevRx; owns equity in Accurius, Enlight, SynDevRx; served on Board of Trustees of Tekla Healthcare Investors, Tekla Life Sciences Investors, Tekla Healthcare Opportunities Fund, and Tekla World Healthcare Fund; and received research grants from Boehringer Ingelheim and Sanofi. Other coauthors have no conflict of interests to declare.

Funding

This work was supported in part by grants from the National Foundation for Cancer Research; the Ludwig Center at Harvard Medical School; the Jane's Trust Foundation; the Nile Albright Research Foundation; and the NIH grants R35-CA197743, R01-CA269672, R01CA259253, U01CA261842, U01-CA224348 and R01-CA208205 to R.K.J.; by the European Research Council grant ERC-2019-CoG-863955 to T.S. and ERC-2022-StG-101076425 to F.M.; by NIH grants GM130830 and GM145362 to F.Y.; and by National Heart, Lung, and Blood Institute grants R01 HL143896, R01 HL059157, and R01 HL127402 to D.M.M.

Data availability statement

All data are included in the Manuscript.

References

- Angeli S, Stylianopoulos T. (2016). Biphasic modeling of brain tumor biomechanics and response to radiation treatment. *J Biomech* 49:1524–31. doi: [10.1016/j.jbiomech.2016.03.029](https://doi.org/10.1016/j.jbiomech.2016.03.029).
- Baluk P, Morikawa S, Haskell A, et al. (2003). Abnormalities of basement membrane on blood vessels and endothelial sprouts in tumors. *Am J Pathol* 163:1801–15. doi: [10.1016/S0002-9440\(10\)63540-7](https://doi.org/10.1016/S0002-9440(10)63540-7).
- Baxter LT, Jain RK. (1989). Transport of fluid and macromolecules in tumors. I. Role of interstitial pressure and convection. *Microvasc Res* 37:77–104. doi: [10.1016/0026-2862\(89\)90074-5](https://doi.org/10.1016/0026-2862(89)90074-5).
- Baxter LT, Jain RK. (1990). Transport of fluid and macromolecules in tumors. II. Role of heterogeneous perfusion and lymphatics. *Microvasc Res* 40:246–63. doi: [10.1016/0026-2862\(90\)90023-k](https://doi.org/10.1016/0026-2862(90)90023-k).
- Baxter LT, Jain RK. (1991a). Transport of fluid and macromolecules in tumors. III. Role of binding and metabolism. *Microvasc Res* 41:5–23. doi: [10.1016/0026-2862\(91\)90003-t](https://doi.org/10.1016/0026-2862(91)90003-t).
- Baxter LT, Jain RK. (1991b). Transport of fluid and macromolecules in tumors. IV. A microscopic model of the perivascular distribution. *Microvasc Res* 41:252–72. doi: [10.1016/0026-2862\(91\)90026-8](https://doi.org/10.1016/0026-2862(91)90026-8).
- Byrne H, Preziosi L. (2003). Modelling solid tumour growth using the theory of mixtures. *Math Med Biol* 20:341–66. doi: [10.1093/imammb/20.4.341](https://doi.org/10.1093/imammb/20.4.341).
- Cabral H, Matsumoto Y, Mizuno K, et al. (2011). Accumulation of sub-100nm polymeric micelles in poorly permeable tumours depends on size. *Nat Nanotechnol* 6:815–23. doi: [10.1038/nnano.2011.166](https://doi.org/10.1038/nnano.2011.166).
- Chauhan VP, Martin JD, Liu H, et al. (2013). Angiotensin inhibition enhances drug delivery and potentiates chemotherapy by decompressing tumour blood vessels. *Nat Commun* 4:2516. doi: [10.1038/ncomms3516](https://doi.org/10.1038/ncomms3516).
- Chauhan VP, Stylianopoulos T, Martin JD, et al. (2012). Normalization of tumour blood vessels improves the delivery of nanomedicines in a size-dependent manner. *Nat Nanotechnol* 7:383–8. doi: [10.1038/nnano.2012.45](https://doi.org/10.1038/nnano.2012.45).
- Chen Y, Huang Y, Li Q, et al. (2023). Targeting Xkr8 via nanoparticle-mediated in situ co-delivery of siRNA and chemotherapy drugs for cancer immunotherapy. *Nat Nanotechnol* 18:193–204. doi: [10.1038/s41565-022-01266-2](https://doi.org/10.1038/s41565-022-01266-2).
- Crist RM, Dasa SSK, Liu CH, et al. (2021). Challenges in the development of nanoparticle-based imaging agents: Characterization and biology. *Wiley Interdiscip Rev Nanomed Nanobiotechnol* 13:e1665. doi: [10.1002/wnan.1665](https://doi.org/10.1002/wnan.1665).
- Dasgupta A, Sofias AM, Kiessling F, Lammers T. (2024). Nanoparticle delivery to tumours: from EPR and ATR mechanisms to clinical impact. *Nat Rev Bioeng* 2:714–6. doi: [10.1038/s44222-024-00203-3](https://doi.org/10.1038/s44222-024-00203-3).
- Deen W. (1987). Hindered transport of large molecules in liquid-filled pores. *AIChE J* 33:1409–25. doi: [10.1002/aic.690330902](https://doi.org/10.1002/aic.690330902).
- Desai N, Trieu V, Yao Z, et al. (2006). Increased antitumor activity, intratumor paclitaxel concentrations, and endothelial cell transport of cremophor-free, albumin-bound paclitaxel, ABI-007, compared with cremophor-based paclitaxel. *Clin Cancer Res* 12:1317–24. doi: [10.1158/1078-0432.CCR-05-1634](https://doi.org/10.1158/1078-0432.CCR-05-1634).
- Evans RC, Quinn TM. (2005). Solute diffusivity correlates with mechanical properties and matrix density of compressed articular cartilage. *Arch Biochem Biophys* 442:1–10. doi: [10.1016/j.abb.2005.07.025](https://doi.org/10.1016/j.abb.2005.07.025).
- Fukumura D, Yuan F, Endo M, Jain RK. (1997). Role of nitric oxide in tumor microcirculation. Blood flow, vascular permeability, and leukocyte-endothelial interactions. *Am J Pathol* 150:713–25.
- Gerlowski LE, Jain RK. (1986). Microvascular permeability of normal and neoplastic tissues. *Microvasc Res* 31:288–305. doi: [10.1016/0026-2862\(86\)90018-x](https://doi.org/10.1016/0026-2862(86)90018-x).
- Hashizume H, Baluk P, Morikawa S, et al. (2000). Openings between defective endothelial cells explain tumor vessel leakiness. *Am J Pathol* 156:1363–80. doi: [10.1016/S0002-9440\(10\)65006-7](https://doi.org/10.1016/S0002-9440(10)65006-7).
- Hobbs SK, Monsky WL, Yuan F, et al. (1998). Regulation of transport pathways in tumor vessels: role of tumor type and microenvironment. *Proc Natl Acad Sci U S A* 95:4607–12. doi: [10.1073/pnas.95.8.4607](https://doi.org/10.1073/pnas.95.8.4607).
- Jain RK, Baxter LT. (1988). Mechanisms of heterogeneous distribution of monoclonal antibodies and other macromolecules in tumors: significance of elevated interstitial pressure. *Cancer Res* 48:7022–32.
- Jain RK, Stylianopoulos T. (2010). Delivering nanomedicine to solid tumors. *Nat Rev Clin Oncol* 7:653–64. doi: [10.1038/nrclinonc.2010.139](https://doi.org/10.1038/nrclinonc.2010.139).
- Kim S-O, Kim J, Okajima T, Cho N-J. (2017). Mechanical properties of paraformaldehyde-treated individual cells investigated by atomic force microscopy and scanning ion conductance microscopy. *Nano Converg* 4:5. doi: [10.1186/s40580-017-0099-9](https://doi.org/10.1186/s40580-017-0099-9).
- Liu X, Lin P, Perrett I, et al. (2017). Tumor-penetrating peptide enhances transcytosis of silicasome-based chemotherapy for pancreatic cancer. *J Clin Invest* 127:2007–18. doi: [10.1172/JCI92284](https://doi.org/10.1172/JCI92284).
- Lu G, Fakurnejad S, Martin BA, et al. (2020). Predicting therapeutic antibody delivery into human head and neck cancers. *Clin Cancer Res* 26:2582–94. doi: [10.1158/1078-0432.CCR-19-3717](https://doi.org/10.1158/1078-0432.CCR-19-3717).
- Matsumura Y, Maeda H. (1986). A new concept for macromolecular therapeutics in cancer chemotherapy: mechanism of tumoritropic accumulation of proteins and the antitumor agent smancs. *Cancer Res* 46:6387–92.
- Mow VC, Kuei SC, Lai WM, Armstrong CG. (1980). Biphasic creep and stress relaxation of articular cartilage in compression? Theory and experiments. *J Biomech Eng* 102:73–84. doi: [10.1115/1.3138202](https://doi.org/10.1115/1.3138202).
- Mpekris F, Angeli S, Pirentis AP, Stylianopoulos T. (2015). Stress-mediated progression of solid tumors: effect of mechanical stress on tissue oxygenation, cancer cell proliferation, and drug delivery. *Biomech Model Mechanobiol* 14:1391–402. doi: [10.1007/s10237-015-0682-0](https://doi.org/10.1007/s10237-015-0682-0).
- Netti PA, Berk DA, Swartz MA, et al. (2000). Role of extracellular matrix assembly in interstitial transport in solid tumors. *Cancer Res* 60:2497–503.
- Papageorgis P, Polydorou C, Mpekris F, et al. (2017). Tranilast-induced stress alleviation in solid tumors improves the efficacy of chemo- and nanotherapeutics in a size-independent manner. *Sci Rep* 7:46140. doi: [10.1038/srep46140](https://doi.org/10.1038/srep46140).
- Pluen A, Boucher Y, Ramanujan S, et al. (2001). Role of tumor-host interactions in interstitial diffusion of macromolecules: cranial vs. subcutaneous tumors. *Proc Natl Acad Sci U S A* 98:4628–33. doi: [10.1073/pnas.081626898](https://doi.org/10.1073/pnas.081626898).
- Polydorou C, Mpekris F, Papageorgis P, et al. (2017). Pirfenidone normalizes the tumor microenvironment to improve chemotherapy. *Oncotarget* 8:24506–17. doi: [10.18632/oncotarget.15534](https://doi.org/10.18632/oncotarget.15534).
- Ramanujan S, Pluen A, McKee TD, et al. (2002). Diffusion and convection in collagen gels: implications for transport in the tumor interstitium. *Biophys J* 83:1650–60. doi: [10.1016/S0006-3495\(02\)73933-7](https://doi.org/10.1016/S0006-3495(02)73933-7).
- Sindhwani S, Syed AM, Ngai J, et al. (2020). The entry of nanoparticles into solid tumours. *Nat Mater* 19:566–75. doi: [10.1038/s41563-019-0566-2](https://doi.org/10.1038/s41563-019-0566-2).

- Skotland T, Sandvig K. (2021). Transport of nanoparticles across the endothelial cell layer. *Nano Today* 36:101029. doi: [10.1016/j.nantod.2020.101029](https://doi.org/10.1016/j.nantod.2020.101029).
- Stewart JM, Schultz DS, Lee O-T, Trinidad ML. (2009a). Collagen cross-links reduce corneal permeability. *Invest Ophthalmol Vis Sci* 50:1606–12. doi: [10.1167/iops.08-2727](https://doi.org/10.1167/iops.08-2727).
- Stewart JM, Schultz DS, Lee O-T, Trinidad ML. (2009b). Exogenous collagen cross-linking reduces scleral permeability: modeling the effects of age-related cross-link accumulation. *Invest Ophthalmol Vis Sci* 50:352–7. doi: [10.1167/iops.08-2300](https://doi.org/10.1167/iops.08-2300).
- Stylianopoulos T, Martin JD, Snuderl M, et al. (2013). Coevolution of solid stress and interstitial fluid pressure in tumors during progression: Implications for vascular collapse. *Cancer Res* 73:3833–41. doi: [10.1158/0008-5472.CAN-12-4521](https://doi.org/10.1158/0008-5472.CAN-12-4521).
- Yuan F, Chen Y, Dellian M, et al. (1996). Time-dependent vascular regression and permeability changes in established human tumor xenografts induced by an anti-vascular endothelial growth factor/vascular permeability factor antibody. *Proc Natl Acad Sci U S A* 93:14765–70. doi: [10.1073/pnas.93.25.14765](https://doi.org/10.1073/pnas.93.25.14765).
- Yuan F, Dellian M, Fukumura D, et al. (1995). Vascular permeability in a human tumor xenograft: molecular size dependence and cutoff size. *Cancer Res* 55:3752–6.
- Yuan F, Leunig M, Berk DA, Jain RK. (1993). Microvascular permeability of albumin, vascular surface area, and vascular volume measured in human adenocarcinoma LS174T using dorsal chamber in SCID mice. *Microvasc Res* 45:269–89. doi: [10.1006/mvre.1993.1024](https://doi.org/10.1006/mvre.1993.1024).
- Yuan F, Salehi HA, Boucher Y, et al. (1994). Vascular permeability and microcirculation of gliomas and mammary carcinomas transplanted in rat and mouse cranial windows. *Cancer Res* 54:4564–8.
- Zhu M, Zhuang J, Li Z, et al. (2023). Machine-learning-assisted single-vessel analysis of nanoparticle permeability in tumour vasculatures. *Nat Nanotechnol* 18:657–66. doi: [10.1038/s41565-023-01323-4](https://doi.org/10.1038/s41565-023-01323-4).

Supporting Information

Fixation alters the physical properties of tumor tissue that regulate nanomedicine transport

John D. Martin^{a,#}, Fotios Mpekris^{b,#}, Vikash P. Chauhan^c, Margaret R. Martin^d, Megan E. Walsh^e, Matthew D. Stuber^f, Donald M. McDonald^g, Fan Yuan^h, Triantafyllos Stylianopoulos^{b,*} and Rakesh K. Jain^{i,*}

Affiliations:

^a*Materia Therapeutics, Las Vegas, NV, USA*

^b*Cancer Biophysics Laboratory, Department of Mechanical and Manufacturing Engineering, University of Cyprus, Nicosia, Cyprus.*

^c*Koch Institute for Integrative Cancer Research, Massachusetts Institute of Technology, Cambridge, MA, USA.*

^d*Department of Computer Science, Tufts University, Medford, MA, USA.*

^e*Department of Chemical Engineering, Carnegie Mellon University, Pittsburgh, PA, USA*

^f*Process Systems and Operations Research Laboratory, Department of Chemical and Biomolecular Engineering, University of Connecticut, Storrs, CT, USA.*

^g*Helen Diller Family Comprehensive Cancer Center, Department of Anatomy, University of California, San Francisco, CA, USA.*

^h*Department of Biomedical Engineering, Duke University, Durham, NC, USA.*

ⁱ*Edwin L. Steele Laboratories, Department of Radiation Oncology, Massachusetts General Hospital, Harvard Medical School, Boston, MA.*

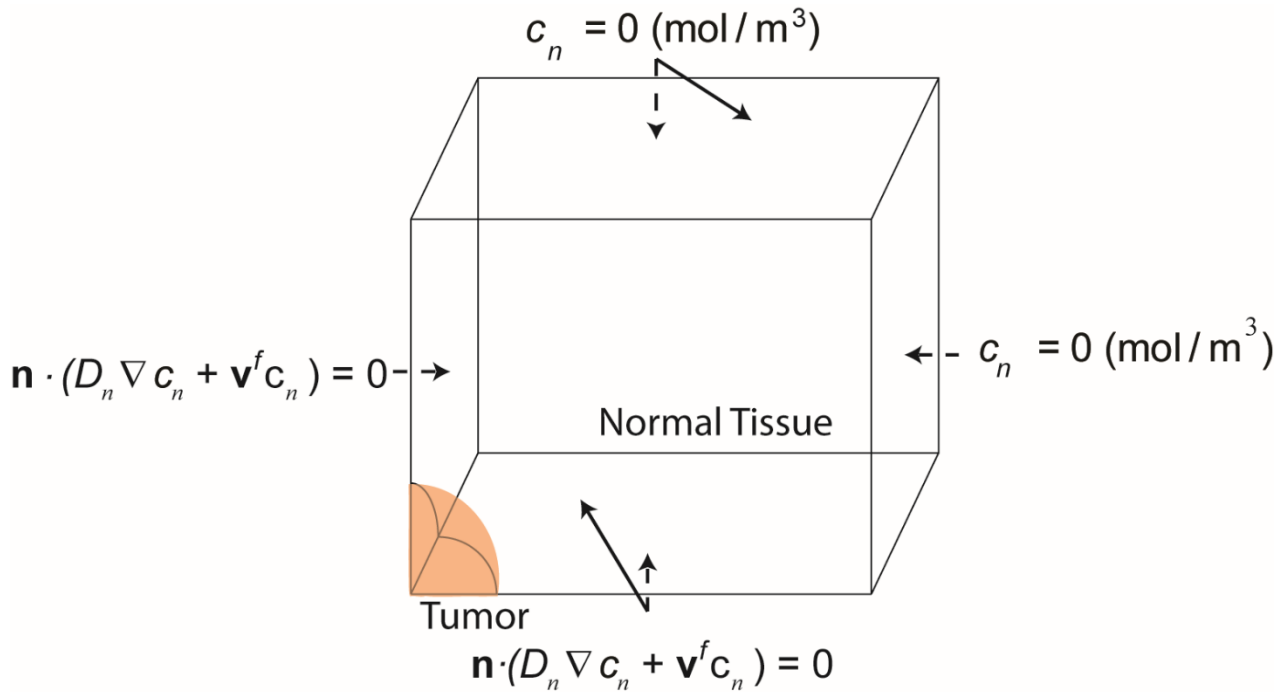
[#]Equal contribution

*Correspondence to: jain@steele.mgh.harvard.edu (RKJ) and tstylian@ucy.ac.cy (TS)

Supplementary Table 1. Parameter values used in the model.

Parameter	Description	Value	Reference
D_n	nanoparticle diffusion coefficient	$4 \times 10^{-7} \text{ cm}^2 \cdot \text{s}^{-1}$ for 15 nm drug; $8 \times 10^{-8} \text{ cm}^2 \cdot \text{s}^{-1}$ for 50 nm drug; $5 \times 10^{-8} \text{ cm}^2 \cdot \text{s}^{-1}$ for 100 nm drug (baseline values)	(Pluen et al., 2001)
L	vessel wall thickness	$5 \times 10^{-6} \text{ m}$	(Stylianopoulos et al., 2013)
P_V	vascular pressure	30 mmHg	(Baxter and Jain, 1989)
η	blood viscosity	$3 \times 10^{-5} \text{ mmHg} \cdot \text{s}$	(Stylianopoulos et al., 2013)
γ	fraction of vessel wall surface area occupied by pores	$1 \times 10^{-3} [-]$	(Chauhan et al., 2012)
S_V	vascular density	34 cm^{-1}	(Sindhwani et al., 2020)
k_{th}	interstitial space hydraulic conductivity	$1 \times 10^{-7} \text{ cm}^2 \cdot \text{mmHg}^{-1} \cdot \text{s}^{-1}$ (baseline value)	(Baxter and Jain, 1989)
a_1	coefficient for K_t	$-73/60 [-]$	(Deen, 1987)
a_2	coefficient for K_t	$77.293/50.400 [-]$	(Deen, 1987)
a_3	coefficient for K_t	$-22.5083 [-]$	(Deen, 1987)
a_4	coefficient for K_t	$-5.617 [-]$	(Deen, 1987)
a_5	coefficient for K_t	$-0.3363 [-]$	(Deen, 1987)
a_6	coefficient for K_t	$-1.216 [-]$	(Deen, 1987)
a_7	coefficient for K_t	$1.647 [-]$	(Deen, 1987)
b_1	coefficient for K_s	$7/60 [-]$	(Deen, 1987)
b_2	coefficient for K_s	$-2.227/50.400 [-]$	(Deen, 1987)
b_3	coefficient for K_s	$4.0180 [-]$	(Deen, 1987)
b_4	coefficient for K_s	$-3.9788 [-]$	(Deen, 1987)
b_5	coefficient for K_s	$-1.9215 [-]$	(Deen, 1987)
b_6	coefficient for K_s	$4.392 [-]$	(Deen, 1987)
b_7	coefficient for K_s	$5.006 [-]$	(Deen, 1987)

Supplementary Figures



Supplementary Figure 1 – Geometry of the computational domain and boundary conditions used in the mathematical model applied to the zombie tumor experiment. We modeled the tumor as a sphere embedded in normal tissue of cubic shape. The radius of the tumor was 6 mm. Because of symmetry, we solved for one-eighth of the domain.

References

- Baxter, L. T., and Jain, R. K. (1989). Transport of fluid and macromolecules in tumors. I. Role of interstitial pressure and convection. *Microvascular Research* 37, 77-104.
- Chauhan, V. P., Stylianopoulos, T., Martin, J. D., Popovic, Z., Chen, O., Kamoun, W. S., Bawendi, M. G., Fukumura, D., and Jain, R. K. (2012). Normalization of tumour blood vessels improves the delivery of nanomedicines in a size-dependent manner. *Nature Nanotechnology* 7, 383-388.
- Deen, W. M. (1987). Hindered Transport of Large molecules in Liquid-Filled Pores. *AIChE J* 33, 1409-1425.
- Pluen, A., Boucher, Y., Ramanujan, S., McKee, T. D., Gohongi, T., di Tomaso, E., Brown, E. B., Izumi, Y., Campbell, R. B., Berk, D. A., and Jain, R. K. (2001). Role of tumor-host interactions in interstitial diffusion of macromolecules: cranial vs. subcutaneous tumors. *Proceedings of the National Academy of Sciences of the United States of America* 98, 4628-4633.
- Sindhvani, S., Syed, A. M., Ngai, J., Kingston, B. R., Maiorino, L., Rothschild, J., MacMillan, P., Zhang, Y., Rajesh, N. U., and Hoang, T. (2020). The entry of nanoparticles into solid tumours. *Nature Materials* 19, 566-575.
- Stylianopoulos, T., Martin, J. D., Snuderl, M., Mpekris, F., Jain, S. R., and Jain, R. K. (2013). Coevolution of solid stress and interstitial fluid pressure in tumors during progression: Implications for vascular collapse. *Cancer research* 73, 3833-3841.